Using optically-pumped magnetometers to measure magnetoencephalographic signals in the human cerebellum

Chin-Hsuan Lin[1], Tim M Tierney[1], Niall Holmes[2], Elena Boto[2], James Leggett[2], Sven Bestmann[1], Richard Bowtell[2], Matthew J Brookes[2], R Chris Miall[3] & Gareth R Barnes[1]

1. Wellcome Centre for Human Neuroimaging, Institute of Neurology, University College London, 12 Queen Square, London, UK
2. Sir Peter Mansfield Imaging Centre, School of Physics and Astronomy, University of Nottingham, Nottingham, UK
3 School of Psychology, University of Birmingham, Birmingham, UK

Abstract

We test the feasibility of an optically pumped magnetometer (OPM)-MEG system for the measurement of human cerebellar activity. We show that the OPM system allows for excellent coverage of this structure by decreasing the average sensor-to-cerebellum distance by around 33% (16mm), compared to a standard MEG helmet. This closer proximity to the cerebellum approximately doubles the signal-to-noise ratio (SNR). As a proof of principle, we used an air-puff stimulus to the eyeball in order to elicit cerebellar evoked and induced responses that are well characterized in non-human models. In three subjects, we observed an evoked component at 50ms post stimulus, which originates in the cerebellum (predominantly ipsilateral). This response was followed by a second component at 100ms post stimulus (predominantly contra-lateral). Sensory stimulation also elicited an event-related broadband spectral power change in the ipsilateral cerebellum at ~100ms in all subjects. We conclude that the OPM-MEG technology offers a promising way to advance the understanding of the information processing mechanisms in the human cerebellum.

Introduction

Our understanding of cerebellar function has undergone a paradigm-shift in recent decades due to the studies of neuroanatomy (Glickstein, Sultan, & Voogd, 2011), neuropsychology (Schmahmann & Sherman, 1998), and functional magnetic resonance imaging (Buckner, 2013; Stoodley & Schmahmann, 2009). Until recently thought of as part of the motor system, accumulating evidence indicates that the cerebellum is essential for a variety of cognitive and social functions (Sokolov, Miall, & Ivry, 2017). Despite this expanding repertoire of cerebellar functions, there is a marked absence of human electrophysiological studies in this area.

In the domain of magnetoencephalography (MEG), less than 1% of publications have reported cerebellar activity (Dalal, Osipova, Bertrand, & Jerbi, 2013). A significant proportion of pioneer work described the cerebellum as one part of physiological (Gross et al., 2002; Jerbi et al., 2007; Muthukumaraswamy et al., 2006; Pollok et al., 2004, 2005; Tass et al., 2003) or pathological (Schnitzler et al., 2009; Timmermann et al., 2003) oscillatory networks, but there have been few subsequent detailed investigations in other domains. This is due to several factors. First, compared to the cerebral cortex, the cerebellar cortex is less favourable to the generation of a measurable MEG signal. This is because its densely folded anatomy causes a

high degree of field attenuation due to locally opposing current sources (Dalal et al., 2013; Hashimoto, Kimura, Tanosaki, Iguchi, & Sekihara, 2003; Tesche & Karhu, 1997). Second, cerebellar neurons are thought to have low firing synchrony based on the small amplitudes observed in local field potential studies (Gerloff, Altenmüller, & Dichgans, 1996). Third, the majority of the cerebellum is situated deep in the human cranium. The relatively large distance from the MEG sensors therefore makes it likely that cerebellar-generated MEG signals will be smaller than those measured due to current flow in the neocortex. Finally, yet importantly, current whole-head MEG systems were designed to target the cerebrum and provide poor coverage of the cerebellum (Ioannides 2005 and **Figure 2 A**). The issue is not exclusive to MEG – to date, few studies with scalp cerebellar EEG have been reported (Lascano et al., 2013; Muthukumaraswamy, Johnson, & Hamm, 2003; Todd, Govender, & Colebatch, 2018). It is widely assumed that scalp EEG recordings for the cerebellum suffer from muscle artefacts (Muthukumaraswamy, 2013). Intracranial recordings in the cerebellum are also scarce because of their limited clinical indications (Dalal et al., 2013; Niedermeyer, 2004). These issues combined mean the electrophysiology of the human cerebellum is almost undocumented.

The development of optically pumped magnetometers (OPMs) provides a new opportunity to investigate cerebellar electrophysiology. OPMs are high sensitivity magnetic field sensors that can be flexibly placed on the scalp and do not need cryogenic cooling so that the sensor-to-brain distance can be significantly reduced. We have recently built such a wearable OPM-MEG system, placing the sensors close to the scalp by mounting them in a 3D printed scanner-cast (Boto et al., 2017, 2018). Currently, these sensors can be positioned in a dense array over a specific brain region of interest (Tierney et al 2018). This system is less susceptible to muscle artefacts compared to EEG (Boto et al., 2018). Moreover, the system is accommodated in a field-nulling apparatus (Holmes et al., 2018) which minimises field variation at the sensors due to head movement in the ambient field. These characteristics make OPM-MEG an ideal candidate for the study of cerebellar electrophysiology that is responsible for both motor and non-motor tasks.

As a proof-of-principle study, we recorded MEG data when non-noxious air-puffs to the eye trigger blinks. Air-puffs are the unconditioned stimuli (US) in a well-established cerebellar learning paradigm: eye-blink conditioning. The stimuli are known to elicit activity in the principal cells of the cerebellum, the Purkinje cells. These cells show “simple spike” responses driven by input from the brainstem pontine nuclei as well as “complex spike” responses to climbing fibres projecting from the inferior olive to bilateral, predominantly ipsilateral, cerebellar cortex, in untrained animals (Ohmae & Medina, 2015). Animals and humans present comparable behaviour, and apparently share similar circuitry and responses to physiological and pathological (lesion) interventions (see Freeman & Steinmetz, 2011 for a review of the system). Functional MRI studies in humans also accord well with corresponding electrophysiological studies in animals, with a prominent BOLD response in ipsilateral

cerebellar cortex (Cheng, Disterhoft, Power, Ellis, & Desmond, 2008; Dimitrova et al., 2002; Thurling et al., 2015).

We aim to demonstrate that air-puff driven neural signals in the cerebellum, which have been observed in both the invasive animal and non-invasive human literature, can be measured with OPM-MEG. We first show the scalp mounted OPM system reduces the sensor-to-cerebellum distance by one-third, which converts into an approximately two-fold increase of signals. We then present both evoked and induced responses measured with OPM-MEG in the cerebellum. Taken together, we show wearable OPM-MEG of the cerebellum provides a promising future to examine the cerebellum during human cognition and action, and pathological conditions linked to cerebellar dysfunction.

Materials and methods:

This section is divided into three parts. First, we describe the OPM-MEG system. Second, we summarise the experimental procedures for cerebellar activity measurement. Finally, we introduce the inversion scheme used to localise the source activity.

Participants

Three healthy subjects (1 female, 2 male) aged 27-50, with no history of psychiatric or neurological diseases, participated in the study. All subjects were naïve to the eye-blink conditioning. The research protocol was approved by the University of Nottingham Medical School Research Ethics Committee and the University of Birmingham Research Ethics Committee. Written informed consent was obtained from all participants. The experiments took place at the University of Nottingham.

OPM-MEG System

The OPM-MEG system has been previously described in detail (Boto et al., 2017, 2018; Holmes et al., 2018; Tierney et al., 2018). Briefly, the system consists of an OPM sensor array within a customised scanner-cast, and a field-nulling apparatus comprising four reference OPM sensors and field-nulling coils (**Figure 1**).

Optically-pumped magnetometer (OPM)

The OPM sensor used here (QuSpin Inc., Louisville, CO, USA) is an integrated unit with a noise level of ~15 fT/√Hz in the 1-100 Hz band, and a dynamic range of ±1.5 nT (for details see (V. K. Shah & Wakai, 2013; V. Shah, Osborne, Orton, & Alem, 2018)). Each OPM sensor head contains a 3 x 3 x 3 mm^3 cell containing a ^{87}Rb vapour, with a 795 nm semiconductor laser beam passing through the cell to pump the atoms to a magnetically sensitive state, and a silicon photodiode. A zero-field resonance is then used to detect the weak biomagnetic fields (Dupont-Roc, Haroche, & Cohen-Tannoudji, 1969). In brief, at zero field the gas is transparent to the laser light and there is maximal signal at the photodiode. Perturbations from zero field cause laser light to be absorbed by the gas (as the atoms have changed energy state) this

changes the transparency of the cell to the laser light, resulting in less signal at the photodiode.

Field nulling apparatus

The Earth's residual static field in the Nottingham magnetically shielded room is ~25nT with a maximal gradient of approximately 10 nT/m. This means that even minimal head movements (e.g. a 4 degree rotation) can easily generate signals which exceed the OPM's dynamic range. In order to mitigate these effects we used a set of bi-planar coils to generate magnetic fields which counteract the remaining static field as measured by four reference sensors close to the head. By applying this method, the dominant component of the static field and field gradient can be diminished by factors of 46 and 13 respectively, in a volume of $40 \times 40 \times 40$ cm^3 encapsulating the head (Boto et al., 2018; Holmes et al., 2018).

Scanner-cast design

Data from an anatomical T1-weighted MRI scan was used to generate a 3D mesh representing the outer surface of each participant's scalp. This 3D mesh was used in 3D printing to shape the inner surface of a nylon head-cast, as described in (Boto et al., 2017; Meyer et al., 2017; Tierney et al., 2018), with sockets around the outer surface to hold the OPM sensors. Importantly, the mesh and subsequently produced scanner-cast provide accurate socket and thus sensor positions and orientations, which are in the same coordinate space of as the MRI image. Therefore, no coregistration is needed and the sensor positions are defined as the centre of the socket bases with a 6.5 mm offset, which takes into account that the sensitive portion of the OPM not being precisely at the base of the sensor. Here, with limited sensors available, we placed the sensors proximal to the cerebellar and somatosensory cortices. **Figure 1** shows the sensor configuration in a typical subject. Across the 3 participants thirteen to nineteen posterior sensors and four to six somatosensory sensors were used. Additionally, two sensors were placed in bilateral infra-orbital slots for eyeblink detection (**Figure 1.A**).

Experiment: Eyeblink paradigm

Eyeblinks were elicited by a 32 ms air-puff delivered through a nozzle mounted on the scanner-cast (**Figure 1.A**); essentially a pressurised air cylinder (1 Bar) fed into a 10 m semi-rigid plastic tube (2mm internal diameter), under the control of a bespoke pneumatic valve controller. Some details of the pneumatic delivery system are given in Leonardelli et al., (2015). The nozzle directed the air-puff to the outer canthus of the left eye from a distance of approximately 2-4 cm, individually adjusted to evoke a visible blink after each delivery, but without discomfort. The arrival time of the air-puff was calibrated off-line using a microphone and was relatively insensitive to distance of the nozzle over a limited range (~1 ms/cm). Subjects received four contiguous 12-minute blocks of stimulation. To equate the task to the baseline phase of a previously validated eyeblink conditioning paradigm (Cheng et al., 2008), each block constituted 200 trials: 140 trials of air-puffs, 50 trials of a 550-ms binaural tone (2800 Hz), and 10 paired trials with the tone co-terminated with air-puff delivery; trial order was randomized in sets of 20. A total of 600 air-puff trials were recorded per subject. Every

trial began with a random wait of 1-2.5 seconds to avoid habituation to puffs; inter-stimulus intervals averaged to 3.6 s.

MEG data collection

The OPM data were digitized at a sampling rate of 1200 Hz, using a 16-bit digital acquisition (DAQ) system (National Instruments, Austin, TX) controlled by custom-written software in LabVIEW.

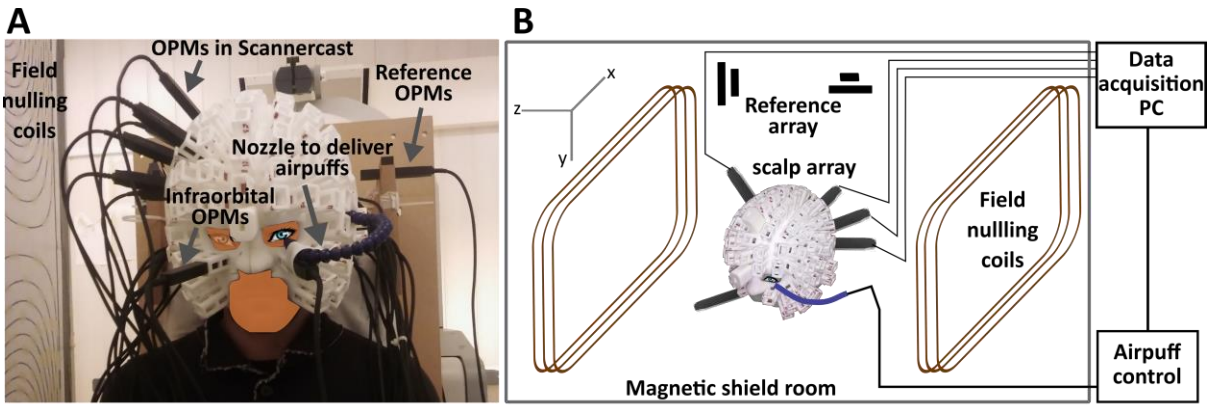

Figure 1. Experimental set-up (A) and schematic illustration (B) of the air-puff paradigm for cerebellar activity measurement. *The participant is seated inside a magnetically shielded room (MSR) wearing a customised scanner-cast. Air-puffs are delivered to the outer canthus of the participant's left eye via a nozzle. OPM sensors are inserted into slots covering the cerebellum and right somatosensory cortex. Two more sensors are placed in bilateral infra-orbital slots to measure eyeblinks. Field-nulling coils stand either side of the participant carrying currents set so as to minimize the residual magnetic field in the MSR, which is measured by 4 reference OPMs prior to scanning. The task-controlling laptop, located outside the MSR, sends synchronizing triggers that were recorded by the data acquisition PC during scanning.*

MEG data analysis

Pre-processing

Data were filtered between 5 and 80 Hz (or 0 and 200 Hz for eye-blink analysis; see Supplementary Material) and each trial epoched between -200 and +500 ms relative to air-puff onset. Because OPMs are configured as magnetometers (as distinct from gradiometers which are used in many cryogenic MEG systems) they are susceptible to increased environmental interference. We mitigated interference by constructing virtual gradiometers, which linearly regress the signal recorded by the reference array from the signal recorded at the scalp array (Boto et al., 2017). Thereafter, data were concatenated across 4 blocks and all 600 trials of data were ranked according to signal variance. Trials with variances higher than [median + 3x median absolute deviation] were rejected (Leys, Ley, Klein, Bernard, & Licata,

2013). For the evoked response analysis, the remaining trials (548, 588 and 585 trials with air-puff stimulation, for subject 1, 2, and 3 respectively) were baseline corrected to the mean of the window 50 ms prior to stimulus onset and then averaged.

For spectral power changes, single trial time-frequency (TF) decompositions in sensor space were calculated for each subject using a Morlet wavelet transform (Tallon-Baudry et al 1998) and then averaged across trials. The wavelet transform was calculated for each time-point between -150 and 450 ms, with 76 scale bins corresponding to frequencies between 5 and 80 Hz. For each trial and frequency, the mean power of the interval from 50 ms before stimulus onset until stimulus presentation was considered as a baseline level. The power change in each frequency band post-stimulus was expressed as the relative percentage change from the pre-stimulus baseline. We additionally calculated the correlations between the latencies of induced power changes and blinks across trials using Pearson's r-values (Yuval-Greenberg at al. 2008): for all trials, the latency of the maximal peak of 5-80 Hz TF data at the time window of 0-350 ms was computed and correlated with the latency of the blink peak (as estimated by the time of the peak amplitude for each trial, examples can be seen in **Supplementary Figure 2.B.**) at the same time window. All of the data analysis was performed using SPM12 within the MATLAB environment (Release 2014a, Mathworks Inc., Natick, MA).

MEG source localisation

We evaluated both the average evoked response using a dipole fit analysis and the average spectral power change using a beamformer. In both cases the volume conductor model was the Nolte single shell model (Nolte, 2003), implemented in SPM12, using the inner-skull boundary from the individual T1-weighted MRI.

Dipole fitting

We reconstructed sources of the evoked field data for each subject using the SPM implementation of variational Bayesian for equivalent current dipole fitting (Kiebel, Daunizeau, Phillips, & Friston, 2008). In brief, the Bayesian inversion scheme assigned prior means and variances of dipole positions and moments. The posterior dipole locations and moments were estimated by maximising the model evidence (as approximated by negative Free energy (Friston, Mattout, Trujillo-Barreto, Ashburner, & Penny, 2007)) for the data, given the model parameters. The advantage of using the Bayesian formalism is that it allows us to test a straightforward set of hypotheses by comparing models in which the sources have different prior locations. We specified the prior mean locations of 4 single dipole models based on the literature (Cheng et al., 2008; Nevalainen, Ramstad, Isotalo, Haapanen, & Lauronen, 2006): (1) right somatosensory cortex (S1, face area), (2) left S1 (face), (3) right cerebellum (in lobule VI) and (4) left cerebellum (lobule VI). Two additional priors in the right and left primary visual cortex (proximal to the cerebellum) were also tested (models 5 and 6). The standard deviation of each prior dipole location was set to 10 mm. The mean and standard deviation of each prior moment were assigned as 0 and 10 nA·m. To avoid local maxima, 50 iterations, with starting locations and orientations randomly sampled from prior

distributions (i.e. the means and standard deviations of prior locations and moments), were carried out for each model in each subject (50 x 6 = 300 iterations in each subject). For each subject we used the model parameters corresponding to the highest free energy value across all iterations. The maximal free energy values across subjects were then averaged.

Beamforming

We used the scalar version of a linear constrained minimum variance beamformer algorithm implemented in the DAISS toolbox for SPM (https://github.com/spm/DAiSS) to localise the source of maximal spectral power change over the brain volume. We used a covariance window of 5 to 80 Hz and -50 to +125 ms and contrasted the 75 to 125 ms post-stimulus period with a pre-stimulus period between -50 and 0 ms. The regularization rate λ was set to be 0 (i.e. unregularized). The source orientation was set in the direction of maximal power. The reconstruction grid spacing was 2 mm. We bootstrapped the analysis in order to find a confidence volume on the global peak estimate by randomly resampling trials with replacement and producing 50 peak estimates per subject.

Results

We first compared the spatial distribution of the OPM sensors around the cerebellum to a standard cryogenic (CTF) MEG system (**Figure 2)** for a typical subject (Subject 2). The cryogenic MEG sensor positions were obtained from another study during which subject 2 underwent conventional MEG scanning (Meyer et al., 2017). It is clear that the coverage of the cryogenic MEG system is sub-optimal for cerebellum (**Figure 2.A**). To provide a fair comparison of the 18 OPM cerebellar sensors, only the nearest 18 SQUID sensors were taken into account. The average sensor-to-cerebellum distance decreased from 49 mm in the SQUID MEG to 33 mm in the OPM-MEG (**Figure 2.B**). This change in distance (factor 1.48) translates into an approximate doubling of the signal magnitude measured by the OPM array, when compared to SQUID sensors. Bespoke scanner-casts could further optimise the placing of sensors for cerebellar recording, by adding another row of sockets below the lowest currently available.

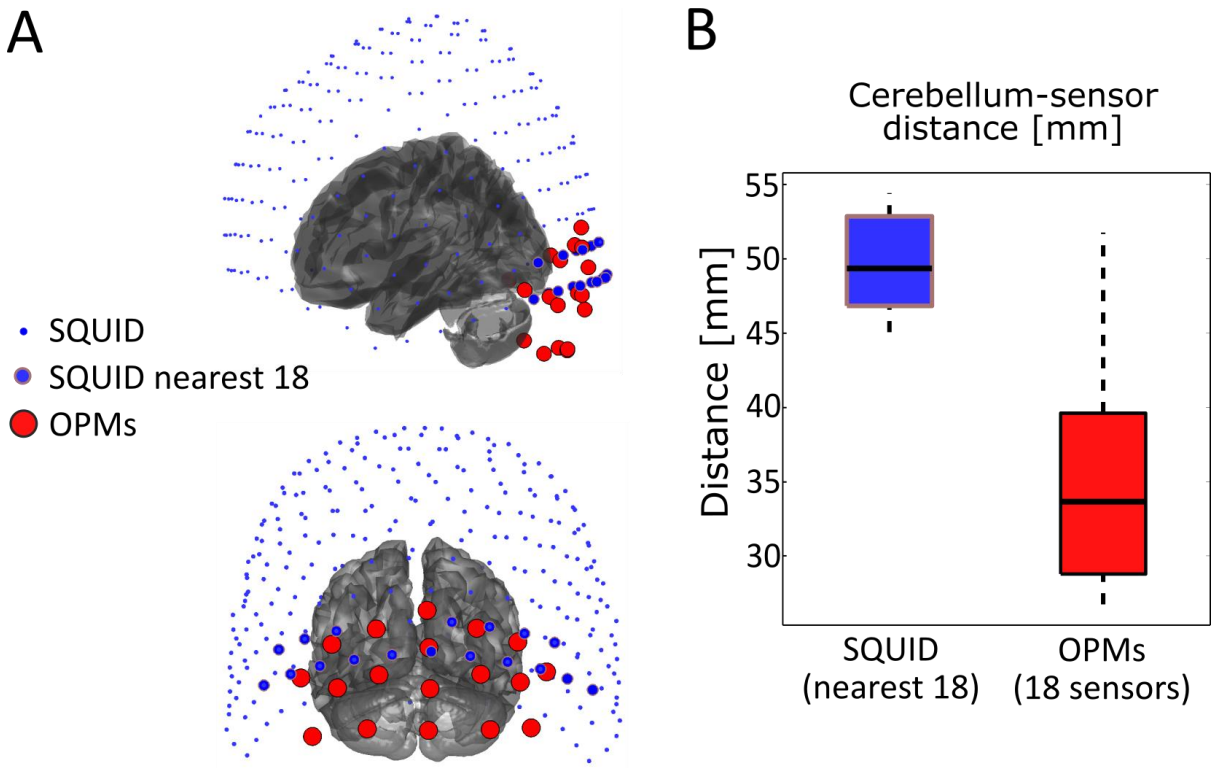

Figure 2. Comparison of the sensor to cerebellum distance for OPM-MEG and SQUID-MEG. *(**A**) The sensor array positions with respect to the brain surface in one subject (subject 2): blue circles: a CTF MEG system with SQUID-based axial gradiometers (VSM MedTech, Vancouver, Canada) and red circles: an OPM sensor array fixed on the scanner-cast. (**B**) Average sensor-to-cerebellum distance (averaged across nearest 18 sensors) reduced by one-third, from 49 mm (SQUID) to 33 mm (OPMs).*

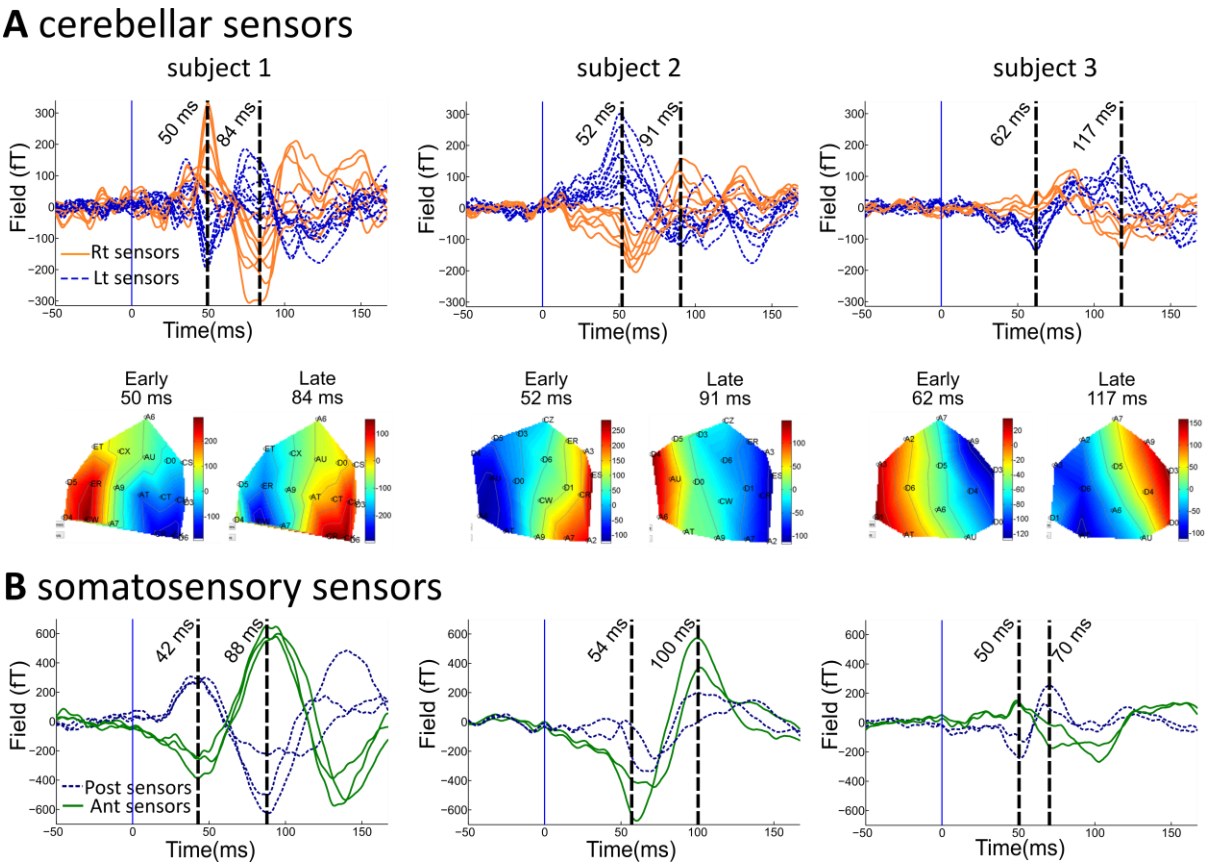

Figure 3 Sensor-level evoked responses following air-puff stimulation. (A) *Upper panel: air-puff evoked responses over the cerebellum for 3 subjects. Each trace corresponds to the average signal for one sensor over the posterior cranium, situated left (blue dashed lines) and right (orange solid lines) of the midline respectively. Lower panel: field maps of the evoked field at the latencies of the two distinct peaks; note different sensor layout for each subject.* ***(B)*** *Sensor-level evoked responses over the right contra-lateral somatosensory area (anterior and posterior sensors as green-solid and blue dotted curves respectively).*

We next looked at the average evoked response to air-puff stimulation on the cerebellar OPM sensors and the sensors positioned over the contra-lateral somatosensory cortex. **Figure 3.A** shows the average evoked response in posterior sensors (left sensors: blue dotted, right sensors: orange solid) for the three subjects. Two main peaks were observed across subjects at around 50-60 ms and 85-115 ms. The field patterns observed at these peaks were qualitatively dipolar (**Figure 3.A** lower panel). There was a slight latency difference (approx. 2 ms on average) between positive and negative going extrema (e.g. Subject 2, **Figure 3.A** upper panel), indicating a more complex source distribution. We also observed two response peaks from sensors proximal to the primary somatosensory cortex (anterior sensors: green solid, posterior: blue dotted, **Figure 3.B**). For each subject, the earliest distinct somatosensory evoked response peaked at 40-50 ms post-stimulus, compatible with the p45m response to facial tactile stimuli (Nevalainen et al., 2006) .

We also looked for event related spectral changes in the cerebellar sensors. **Figure 4** shows the average time-frequency spectrograms (in percentage change of power) for the sensor

with the largest power change in each subject. Increased broadband activity, peaking at ~100 ms post puff contact can be seen in all three subjects. The peak correlation between the latencies of the maximal power changes and blinks, across trials, was significant ($p<0.001$ in all cases) although weak (R Square = 0.02, 0.02, 0.03 for the three subjects, also see **Supplementary Figure 2**).

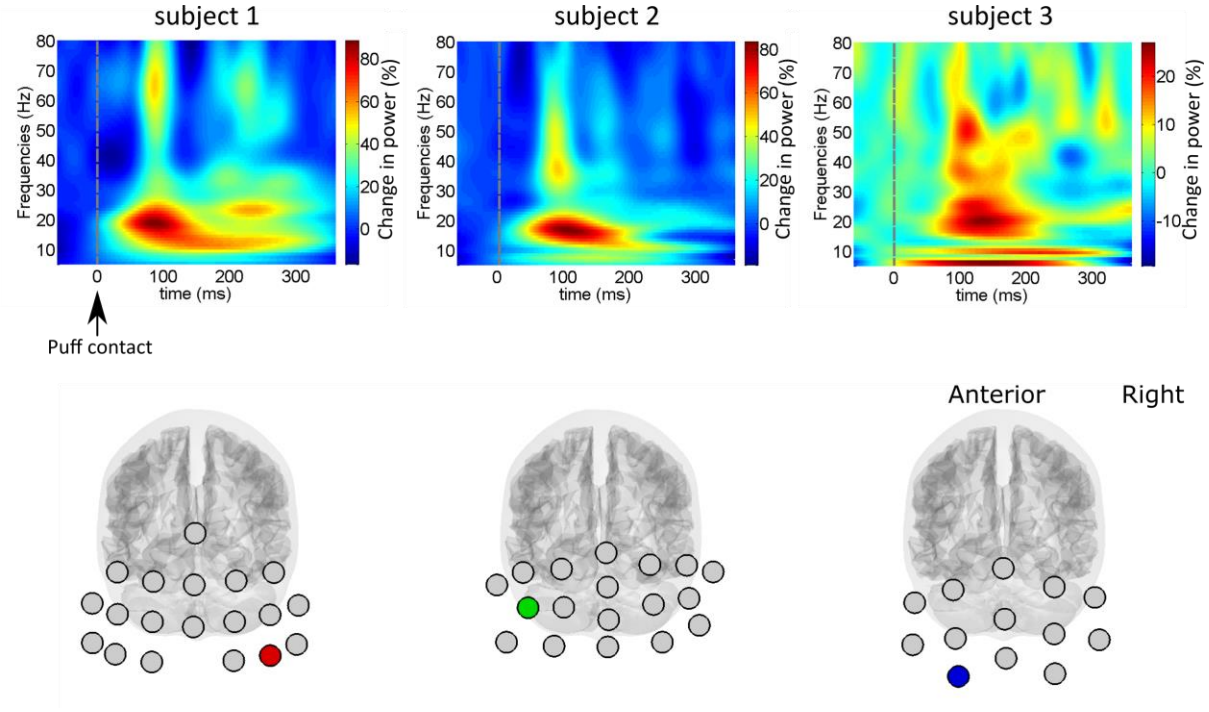

Figure 4 *Time-frequency spectrograms showing event related spectral changes to air-puff stimulation. Each panel is each subject's average across all trials at the sensor with the maximal power change. The positions of these sensors are marked as coloured circles for each subject and mapped onto the MNI template brain (lower panel).*

Source reconstruction

Figure 5 shows the source reconstruction results of early and late evoked responses. **Figure 5.A** compares the free energy values for the early response (50-60ms; top panel) and late responses (85-115ms, bottom panel) for six models with different source location priors, averaged across subjects. Both cerebellar priors are significantly better than the other models ($\Delta F > 3$, as F approximates the log likelihood, a positive difference of 3 means the preferable model is about twenty times more likely). The left (ipsilateral) cerebellum lobule VI had the highest model evidence for both peaks; although this model was not significantly better than the model of a source in the right cerebellum ($\Delta F = 0.8$ for early and 2.2 for late peaks). **Figure 5.B** shows the fitted source locations for subject-specific, early and late time-windows. The source localisations were within the cerebellum or the brainstem/cerebellar peduncle adjacent to the cerebellum. Table 1 shows the MNI coordinates and anatomical labels of each fit.

Dipole locations converged into the cerebellum even when using priors in the occipital lobe (model 5 & 6, see **Figure 5.C.**). We also undertook an additional Bayesian single dipole fit using an uninformative prior (initial location randomly sampled from a distribution centring at the middle point of the cerebellum with a 50-mm standard deviation; **Figure 5.D.**) and found similar results.

In order to locate the event-related power changes we used a beamformer with a covariance window covering a time range of -50 to +125 ms relative to air-puff onset, and a 5-80 Hz frequency band. We contrasted the power within this band between time windows of +75 to +125 ms and -50 to 0 ms relative to baseline (based on the observed sensor level power changes, **Figure 4**). We plotted each subject's global maximum location and the bootstrapped confidence volume in the MNI space in **Figure 6**. The locations were in the left (ipsilateral) cerebellum in all 3 subjects. The 95% confidence volumes based on 50 bootstraps were lower than the grid spacing (2 mm) for subject 1 and 2 and was 12.0 mm^3 for subject 3.

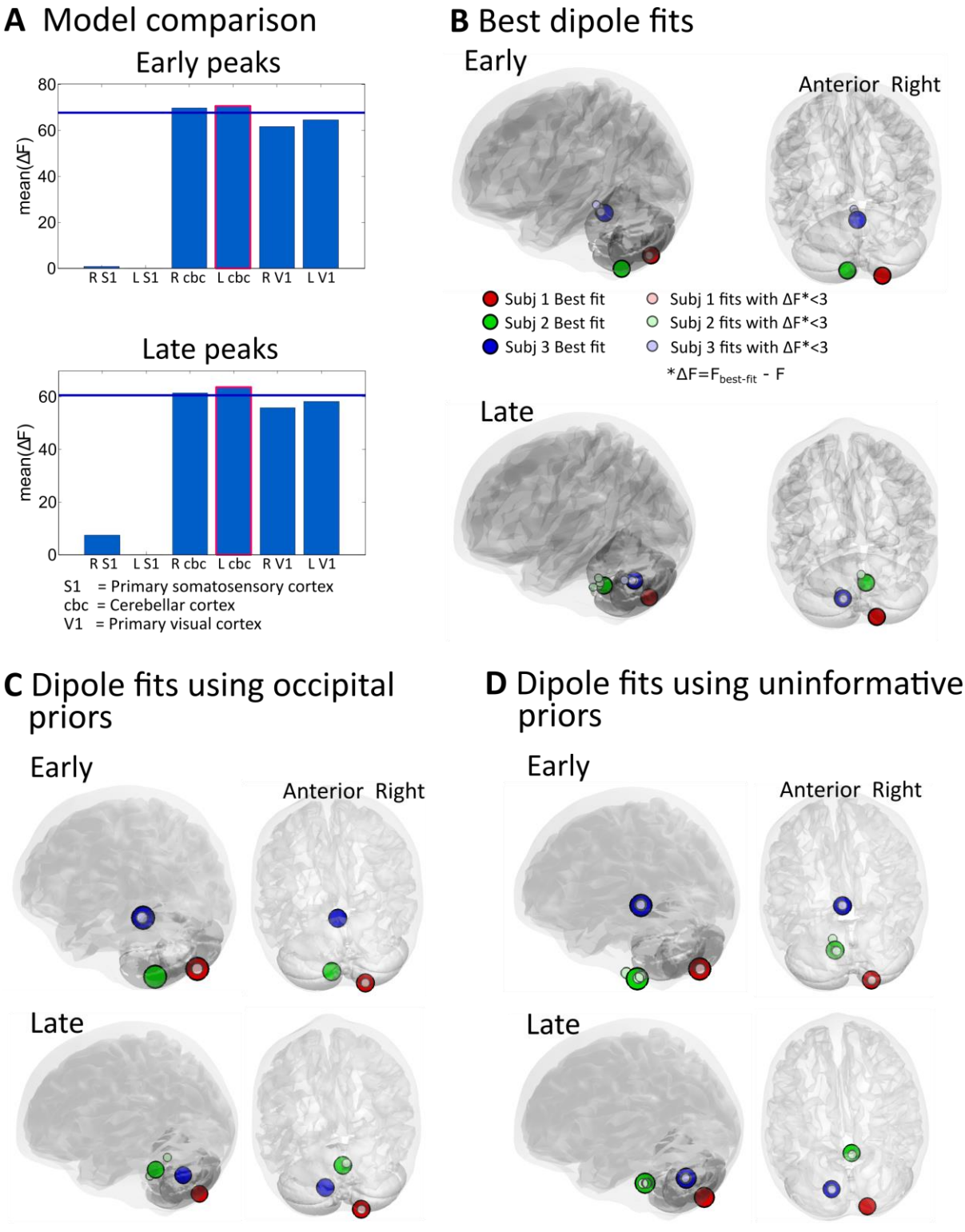

Figure 5 Evoked response source localisation: Single dipole fits using subject-specific early and late peaks of evoked responses. ***(A)*** *Bayesian model comparison. Free energy (F) is used to approximate the model evidence of a given source solution. Bars represent the mean Free energy value relative to the poorest model (which was Left S1 both early and late peaks). The left (ipsilateral) cerebellum has the highest model evidence for both early and late peaks. It should also be noted that both the left and right cerebellum are significantly better than the*

*other priors (ΔF > 3, blue line). **(B)** Single dipole fits for each participant. Large circles represent the source locations of models with highest evidence for each individual. Smaller circles are models which are suboptimal but not significantly so (ΔF = $F_{best\text{-}fit}$ - F < 3). **(C)** Single dipole fits for each peak and subject when using priors in either left or right occipital lobe **(D)** Single dipole fits for each peak and subject using an effectively uninformative prior (in centre of cerebellum with standard deviation 50 mm). As in **(B)**, large circles in both **(C)** and **(D)** represent the best fits for each subjects and small circles represent fits which have ΔF = $F_{best\text{-}fit}$ - F < 3. The Bayes' posterior estimates of source positions in **(C)** and **(D)** are largely in agreement with the dipole fits using more carefully selected physiological priors in **(B)**.*

	Early				Late			
	Location•	MNI coordinates			Location	MNI coordinates		
		X	Y	Z		X	Y	Z
Subject 1	R VIII	17.95	-72.7	-55	R VIII	12.34	-71.1	-52.1
Subject 2	L IX	-7.71	-55.3	-61	R pons	8.4	-38.07	-43.62
Subject 3	R cerebellar peduncle	2.32	-40.85	-21.7	L deep nucleus	-14	-64.63	-35.2

Table 1. Location of dipole fits for early and late components of the evoked response in 3 subjects. Location labels were based on (Diedrichsen, Balsters, Flavell, Cussans, & Ramnani, 2009).

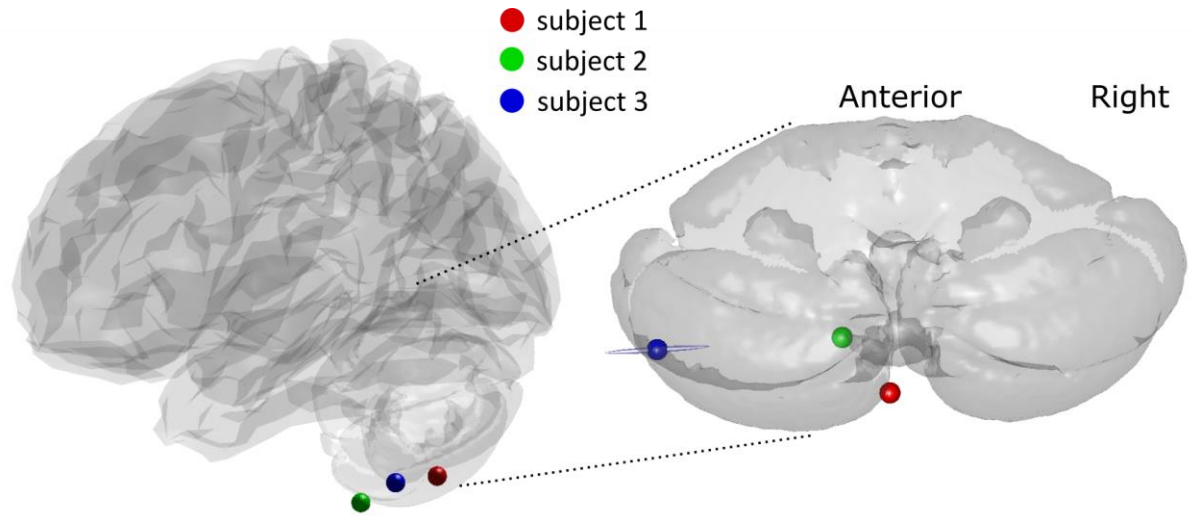

***Figure 6 Beamformer source localisation.** The source locations of subject specific global maximal power change at the time window 75-125 ms are all in the left, i.e. ipsilateral, cerebellum. The light-blue ellipsoid is the 95% confidence volume for Subject 3 estimated by*

50 bootstraps. Confidence volumes for Subjects 1 & 2 are smaller than the 2 mm beamformer grid spacing.

Discussion

We have demonstrated that a small (less than 20 sensor) OPM array can detect cerebellar activity during unconditioned eyeblinks elicited by brief air puffs. The evoked responses had both early (~50 ms) and late components (~90-110 ms); spectrally we found a broad-band power change at ~100 ms. The source localisation for both evoked and event-related spectral change was generally consistent with previous neural recordings in animals and fMRI in humans (i.e. ipsilateral).

Evoked fields from the cerebellum used to be considered unattainable at the scalp level because low-amplitude cerebellar activity would be concealed by stronger adjacent neocortical activity. In the small number of published MEG studies, cerebellar activation to somatosensory stimuli has been identified by either using *a priori* assumptions of an equivalent current dipole (ECD) in the cerebellum (Tesche & Karhu, 1997; Tesche & Karhu, 2000) or by using a beamforming source reconstruction (Hashimoto et al., 2003). The Hashimoto study (Hashimoto et al., 2003) showed a four-component response in the cerebellum following median nerve stimulation, and the authors made putative assignment of these peaks to different cerebellar inputs. The Hashimoto showed robust source level images (again lateralized stimuli predominantly localized to medial cerebellum) but based on 10,000 trials. By contrast, our results are apparent at sensor level and are based on 550-580 trials per participant. We anticipate that a further reduction in required trials could be achieved by bespoke design of a cerebellar scanner-cast, to optimise sensor locations and further increase SNR.

We were concerned about the contribution of artefacts from non-neural sources, especially the neck muscles and eye movements. The corneo-retinal dipole or extra-orbital muscle is not likely to be an issue, as this type of artefact has been shown to be highly focal and limited to fronto-central sensors (Carl, Açik, König, Engel, & Hipp, 2012; Muthukumaraswamy, 2013). Likewise, the air-puff induced eye-blink occurs relatively late (~100 ms) after stimulus onset (**Supplementary Figure 1)** making it an unlikely source of the early transients. For the same reason, we think it unlikely that the observed changes could be due to some reflexive head/neck muscle activity, as we would expect this to occur post-eyeblink (Valls-Solé et al. 1999). For induced response, the significant, but only weak temporal correlation between the latencies of spectral power changes and blinks (explaining less than 4% of the variance in latency) suggested they were not blink-related artefacts either (**Supplementary Figure 2).** Further, we observed the same spectral profile (**Supplementary Figure 3**) at the source level (using an unregularized beamformer) which we would not have expected if the response were due to muscle artefact (Hipp & Siegel, 2013). However, it is important to note that while blink-related non-neural sources can generally be excluded, the cerebellum is known to be a key part of the blink-control circuit (Hesslow, 1994).

To our knowledge, this is the first MEG study to examine the neural response due to the unconditioned stimulus (US, i.e. air-puffs) of eyeblink conditioning. Being a model system for cerebellar learning, the neural circuits of both unconditioned and conditioned blink responses have been extensively investigated in animals. In untrained rodents, single-unit recording from Purkinje cells in ipsilateral cerebellar cortical lobule VI show that air-puffs elicit climbing fibre inputs, with high probability, peaking around 15-50 ms post-stimulus (Mostofi, Holtzman, Grout, Yeo, & Edgley, 2010; Ohmae & Medina, 2015). Importantly, excitation of the very powerful climbing fibre-Purkinje cell synapse, simultaneously activating the dendrites of a spatially aligned set of Purkinje cells has been considered to be the most probable source for a strong open field detected by MEG recordings (Tesche & Karhu, 1997). According to animal local field potential recording, the US reaches the cerebellum first via an early mossy fibre response and then the aforementioned climbing fibre response (Hesslow, 1994; Mostofi et al., 2010). Our MEG evoked responses showed two peaks, the first tightly clustered around 50-60 ms while the second occurred 80-110 ms post-puff with significant inter-individual differences in latency. These first human data are thus broadly consistent with the animal literature. Previously, similar qualitative features including multiple components (Hashimoto et al., 2003; Tesche & Karhu, 2000) and inter-individual latency variability (Tesche & Karhu, 1997) responding to simple somatosensory input have also been found in human MEG at source levels.

We also report a broadband power increase ranging ~100 ms following air-puff stimulation in all subjects, originating from the ipsilateral cerebellum. In the sparse number of MEG studies reporting cerebellar oscillatory changes, Tesche and colleagues discovered increases in the alpha and gamma range power in response to somatosensory stimulation administration and omission (Tesche & Karhu, 2000). For action execution and observation, decreased power in alpha and beta range was observed (Kennedy, Singh, & Muthukumaraswamy, 2011; Muthukumaraswamy et al., 2006).

The Bayesian inversion scheme found the left (ipsilateral) lobule VI was the best fitting single-dipole model of these evoked responses. For the induced response, the left cerebellum was also identified as the neuronal source by beamforming. The source locations are in agreement with previous findings (Cheng et al., 2008). However, it should be noted that in all three subjects, the best evoked-response fits located close to the midline, more medial than lobule VI. Besides, for both early and late peaks of the evoked field, the differences of Free energy values between the right and left cerebellum lobule VI were small ($\Delta F < 3$, **Figure 5.A**). One potential cause of this finding is that although ipsilateral lobule VI is the dominant neuronal source of the US signal, concurrent (but weaker) neuronal activation has been found in the contralateral lobule VI in both human fMRI (Dimitrova et al., 2002; Thurling et al., 2015) and in animal studies (Mostofi et al., 2010). When fitting evoked fields with two-dipole priors, the majority of best fits were indeed paired bilateral cerebellar sources (see **Supplementary Figure 4**). These results support the hypothesis of bilateral activation in the cerebellum by unilateral air-puff stimulation. This said, we admit the current results cannot conclusively

locate the sources at a resolution of cerebellar lobules (Schmahmann et al., 1999). To give confidence in the identities and localisations of our findings, we intend to extend the studies to include classical conditioning and extinction of the eye-blink, and to track the predicted changes in the responses to the unconditioned and conditioned stimuli.

The current sensor layout is limited by the number of OPM sensors available. Given the relatively greater depth of the cerebellum, its complex architecture, and the diffuse spatial signature seen in the evoked responses (see the fieldmaps in the **Figure 3.A.**, lower panel), the source localisation would likely benefit from a denser and spatially extended sensor coverage. Additionally, it would be useful to design scanner-casts allowing sensor placed over the upper neck to provide a necessary scope on the inferior cerebellum, which was less sufficiently covered by the current set-up (see **Figure 2.A.**).

Conclusion

We have demonstrated an OPM-MEG system that can be used to study the electrophysiology of the human cerebellum. The similarities between human MEG and animal field potential data in this proof-of-principle task offers promise for future studies to advance our understanding of cerebellar function through non-invasive electrophysiology in humans. Possessing sufficient signal detectability and being wearable and potentially moveable, we expect OPM-MEG systems to be a powerful tool in the investigation of cerebellar functions in both motor and cognitive tasks (Boto et al., 2018; Sokolov et al., 2017; Tierney et al., 2018). This OPM-MEG system also has the capacity to fill the “white regions” (Niedermeyer, 2004; Schomer & Lopes da Silva, 2010) of the map of clinical electrophysiology in the cerebellum, with impacts on diseases including movement disorders (Bostan & Strick, 2018), mental disorders (Romer et al., 2017), dementia (Fyfe, 2016), to name a few.

Acknowledgements

CL is funded by a BBSRC research grant (BB/M009645/1). This work was supported by a Wellcome collaborative award to GRB, MJB and RB (203257/Z/16/Z, 203257/B/16/Z). The WCHN is supported by a strategic award from Wellcome (091593/Z/10/Z). RCM is funded by a Royal Society Leverhulme Senior Fellowship and by Wellcome grant WT212422. We thank Uta Noppeney for use of the pneumatic controller to deliver air-puffs and Jose David Lopez for helpful discussion.

References:

Bostan, A. C., & Strick, P. L. (2018). The basal ganglia and the cerebellum: Nodes in an integrated network. *Nature Reviews Neuroscience*, *19*(6), 338–350. https://doi.org/10.1038/s41583-018-0002-7

Boto, E., Holmes, N., Leggett, J., Roberts, G., Shah, V., Meyer, S. S., … Brookes, M. J. (2018). Moving magnetoencephalography towards real-world applications with a wearable system. *Nature*, *555*(7698), 657–661. https://doi.org/10.1038/nature26147

Boto, E., Meyer, S. S., Shah, V., Alem, O., Knappe, S., Kruger, P., … Brookes, M. J. (2017). A new generation of magnetoencephalography: Room temperature measurements using optically-pumped magnetometers. *NeuroImage*, *149*(January), 404–414. https://doi.org/10.1016/j.neuroimage.2017.01.034

Buckner, R. L. (2013). The cerebellum and cognitive function: 25 years of insight from anatomy and neuroimaging. *Neuron*, *80*(3), 807–815. https://doi.org/10.1016/j.neuron.2013.10.044

Carl, C., Açik, A., König, P., Engel, A. K., & Hipp, J. F. (2012). The saccadic spike artifact in MEG. *NeuroImage*, *59*(2), 1657–1667. https://doi.org/10.1016/j.neuroimage.2011.09.020

Cheng, D. T., Disterhoft, J. F., Power, J. M., Ellis, D. A., & Desmond, J. E. (2008). Neural substrates underlying human delay and trace eyeblink conditioning. *Proceedings of the National Academy of Sciences*, *105*(23), 8108–8113. https://doi.org/10.1073/pnas.0800374105

Dalal, S. S., Osipova, D., Bertrand, O., & Jerbi, K. (2013). Oscillatory activity of the human cerebellum: The intracranial electrocerebellogram revisited. *Neuroscience and Biobehavioral Reviews*, *37*(4), 585–593. https://doi.org/10.1016/j.neubiorev.2013.02.006

Diedrichsen, J., Balsters, J. H., Flavell, J., Cussans, E., & Ramnani, N. (2009). A probabilistic MR atlas of the human cerebellum. *NeuroImage*, *46*(1), 39–46. https://doi.org/10.1016/j.neuroimage.2009.01.045

Dimitrova, A., Weber, J., Maschke, M., Elles, H. G., Kolb, F. P., Forsting, M., … Timmann, D. (2002). Eyeblink-related areas in human cerebellum as shown by fMRI. *Human Brain Mapping*, *17*(2), 100–115. https://doi.org/10.1002/hbm.10056

Dupont-Roc, J., Haroche, S., & Cohen-Tannoudji, C. (1969). Detection of very weak magnetic fields (10−9gauss) by 87Rb zero-field level crossing resonances. *Physics Letters A*, *28*(9), 638–639. https://doi.org/10.1016/0375-9601(69)90480-0

Freeman, J. H., & Steinmetz, A. B. (2011). Neural circuitry and plasticity mechanisms underlying delay eyeblink conditioning. *Learning & Memory*, *18*(10), 666–677. https://doi.org/10.1101/lm.2023011

Friston, K., Mattout, J., Trujillo-Barreto, N., Ashburner, J., & Penny, W. (2007). Variational free energy and the Laplace approximation. *NeuroImage*, *34*(1), 220–234. https://doi.org/10.1016/j.neuroimage.2006.08.035

Fyfe, I. (2016). Dementia: Cerebellar atrophy has disease-specific patterns. *Nature Reviews Neurology*, *12*(4), 188. https://doi.org/10.1038/nrneurol.2016.28

Gerloff, C., Altenmüller, E., & Dichgans, J. (1996). Disintegration and reorganization of cortical motor processing in two patients with cerebellar stroke. *Electroencephalography and Clinical Neurophysiology*, *98*(1), 59–68. https://doi.org/10.1016/0013-4694(95)00204-9

Glickstein, M., Sultan, F., & Voogd, J. (2011). Functional localization in the cerebellum. *Cortex*, *47*(1), 59–80. https://doi.org/10.1016/j.cortex.2009.09.001

Gross, J., Timmermann, L., Kujala, J., Dirks, M., Schmitz, F., Salmelin, R., & Schnitzler, A. (2002). The neural basis of intermittent motor control in humans. *Proceedings of the National Academy of Sciences of the United States of America*, *99*(4), 2299–2302. https://doi.org/10.1073/pnas.032682099

Hashimoto, I., Kimura, T., Tanosaki, M., Iguchi, Y., & Sekihara, K. (2003). Muscle afferent inputs from the hand activate human cerebellum sequentially through parallel and climbing fiber systems. *Clinical Neurophysiology*, *114*(11), 2107–2117. https://doi.org/10.1016/S1388-2457(03)00233-5

Hesslow, G. (1994). Correspondence between climbing fibre input and motor output in eyeblink related areas in cat cerebellar cortex. *The Journal of Physiology*, *476*(2), 229–244. https://doi.org/10.1113/jphysiol.1994.sp020126

Holmes, N., Leggett, J., Boto, E., Roberts, G., Hill, R. M., Tierney, T. M., … Bowtell, R. (2018). A bi-planar coil system for nulling background magnetic fields in scalp mounted magnetoencephalography. *NeuroImage*. https://doi.org/10.1016/j.neuroimage.2018.07.028

Jerbi, K., Lachaux, J.-P., N'Diaye, K., Pantazis, D., Leahy, R. M., Garnero, L., & Baillet, S. (2007). Coherent neural representation of hand speed in humans revealed by MEG imaging. *Proceedings of the National Academy of Sciences*, *104*(18), 7676–7681. https://doi.org/10.1073/pnas.0609632104

Kennedy, J. S., Singh, K. D., & Muthukumaraswamy, S. D. (2011). An MEG investigation of the neural mechanisms subserving complex visuomotor coordination. *International Journal of Psychophysiology*, *79*(2), 296–304. https://doi.org/10.1016/j.ijpsycho.2010.11.003

Kiebel, S. J., Daunizeau, J., Phillips, C., & Friston, K. J. (2008). Variational Bayesian inversion of the equivalent current dipole model in EEG/MEG. *NeuroImage*, *39*(2), 728–741. https://doi.org/10.1016/j.neuroimage.2007.09.005

Kirsch, P., Achenbach, C., Kirsch, M., Heinzmann, M., Schienle, A., & Vaitl, D. (2003). Cerebellar and hippocampal activation during eyeblink conditioning depends on the experimental paradigm: A MEG Study. *Neural Plasticity*, *10*(4), 291–301. https://doi.org/10.1155/NP.2003.291

Lascano, A. M., Lemkaddem, A., Granziera, C., Korff, C. M., Boex, C., Jenny, B., … Vulliemoz, S. (2013). Tracking the source of cerebellar epilepsy: Hemifacial seizures associated with cerebellar cortical dysplasia. *Epilepsy Research*, *105*(1–2), 245–249.

https://doi.org/10.1016/j.eplepsyres.2012.12.010

Leonardelli, E., Braun, C., Weisz, N., Lithari, C., Occelli, V., & Zampini, M. (2015). Prestimulus oscillatory alpha power and connectivity patterns predispose perceptual integration of an audio and a tactile stimulus. *Human Brain Mapping*, *36*(9), 3486–3498. https://doi.org/10.1002/hbm.22857

Leys, C., Ley, C., Klein, O., Bernard, P., & Licata, L. (2013). Detecting outliers: Do not use standard deviation around the mean, use absolute deviation around the median. *Journal of Experimental Social Psychology*, *49*(4), 764–766. https://doi.org/10.1016/j.jesp.2013.03.013

Meyer, S. S., Bonaiuto, J., Lim, M., Rossiter, H., Waters, S., Bradbury, D., … Barnes, G. R. (2017). Flexible head-casts for high spatial precision MEG. *Journal of Neuroscience Methods*, *276*, 38–45. https://doi.org/10.1016/j.jneumeth.2016.11.009

Mostofi, A., Holtzman, T., Grout, A. S., Yeo, C. H., & Edgley, S. A. (2010). Electrophysiological Localization of Eyeblink-Related Microzones in Rabbit Cerebellar Cortex. *Journal of Neuroscience*, *30*(26), 8920–8934. https://doi.org/10.1523/JNEUROSCI.6117-09.2010

Muthukumaraswamy, S. D. (2013). High-frequency brain activity and muscle artifacts in MEG/EEG: a review and recommendations. *Frontiers in Human Neuroscience*, *7*(April), 1–11. https://doi.org/10.3389/fnhum.2013.00138

Muthukumaraswamy, S. D., Johnson, B. W., Gaetz, W. C., & Cheyne, D. O. (2006). Neural processing of observed oro-facial movements reflects multiple action encoding strategies in the human brain. *Brain Research*, *1071*(1), 105–112. https://doi.org/10.1016/j.brainres.2005.11.053

Muthukumaraswamy, S. D., Johnson, B. W., & Hamm, J. P. (2003). A high density ERP comparison of mental rotation and mental size transformation. *Brain and Cognition*, *52*(2), 271–280. https://doi.org/10.1016/S0278-2626(03)00077-0

Nevalainen, P., Ramstad, R., Isotalo, E., Haapanen, M. L., & Lauronen, L. (2006). Trigeminal somatosensory evoked magnetic fields to tactile stimulation. *Clinical Neurophysiology*, *117*(9), 2007–2015. https://doi.org/10.1016/j.clinph.2006.05.019

Niedermeyer, E. (2004). The electrocerebellogram. *Clinical EEG and Neuroscience : Official Journal of the EEG and Clinical Neuroscience Society (ENCS)*, *35*(2), 112–115.

Nolte, G. (2003). The magnetic lead field theorem in the quasi-static approximation and its use for magnetoenchephalography forward calculation in realistic volume conductors. *Physics in Medicine and Biology*, *48*(22), 3637–3652. https://doi.org/10.1088/0031-9155/48/22/002

Ohmae, S., & Medina, J. F. (2015). Climbing fibers encode a temporal-difference prediction error during cerebellar learning in mice. *Nature Neuroscience*, *18*(12), 1798–1803. https://doi.org/10.1038/nn.4167

Pollok, B., Gross, J., Dirks, M., Timmermann, L., & Schnitzler, A. (2004). The cerebral oscillatory network of voluntary tremor. *Journal of Physiology*, *554*(3), 871–878. https://doi.org/10.1113/jphysiol.2003.051235

Pollok, B., Gross, J., Müller, K., Aschersleben, G., & Schnitzler, A. (2005). The cerebral oscillatory network associated with auditorily paced finger movements. *NeuroImage*, *24*(3), 646–655. https://doi.org/10.1016/j.neuroimage.2004.10.009

Romer, A. L., Knodt, A. R., Houts, R., Brigidi, B. D., Moffitt, T. E., Caspi, A., & Hariri, A. R. (2017). Structural alterations within cerebellar circuitry are associated with general liability for common mental disorders. *Molecular Psychiatry*, (February 2017), 1084–1090. https://doi.org/10.1038/mp.2017.57

Schmahmann, J. D., Doyon, J., McDonald, D., Holmes, C., Lavoie, K., Hurwitz, A., … Petrides, M. (1999). Three-dimensional MRI atlas of the human cerebellum in proportional stereotaxic space. *NeuroImage*, *10*(3 I), 233–260. https://doi.org/10.1006/nimg.1999.0459

Schmahmann, J. D., & Sherman, J. C. (1998). The cerebellar cognitive affective syndrome. *Brain*, *121*(4), 561–579. https://doi.org/10.1093/brain/121.4.561

Schnitzler, A., Münks, C., Butz, M., Timmermann, L., & Gross, J. (2009). Synchronized brain network associated with essential tremor as revealed by magnetoencephalography. *Movement Disorders*, *24*(11), 1629–1635. https://doi.org/10.1002/mds.22633

Schomer, D. L., & Lopes da Silva, F. H. (2010). *Electroencephalography. Basic principles, clinical applications, and related fields* (6th ed.). Lippincott Williams & Wilkins, Philadelphia, PA, USA.

Shah, V. K., & Wakai, R. T. (2013). A compact, high performance atomic magnetometer for biomedical applications. *Physics in Medicine and Biology*, *58*(22), 8153–8161. https://doi.org/10.1088/0031-9155/58/22/8153

Shah, V., Osborne, J., Orton, J., & Alem, O. (2018). Fully integrated, standalone zero field optically pumped magnetometer for biomagnetism. *Steep Dispersion Engineering and Opto-Atomic Precision Metrology XI*, (February), 51. https://doi.org/10.1117/12.2299197

Sokolov, A. A., Miall, R. C., & Ivry, R. B. (2017). The Cerebellum: Adaptive Prediction for Movement and Cognition. *Trends in Cognitive Sciences*, *21*(5), 313–332. https://doi.org/10.1016/j.tics.2017.02.005

Stoodley, C. J., & Schmahmann, J. D. (2009). Functional topography in the human cerebellum: A meta-analysis of neuroimaging studies. *NeuroImage*, *44*(2), 489–501. https://doi.org/10.1016/j.neuroimage.2008.08.039

Tallon-Baudry, C., Bertrand, O., Peronnet, F., & Pernier, J. (1998). Induced gamma-band activity during the delay of a visual short-term memory task in humans. *The Journal of Neuroscience : The Official Journal of the Society for Neuroscience*, *18*(11), 4244–4254. https://doi.org/20026318

Tass, P. A., Fieseler, T., Dammers, J., Dolan, K., Morosan, P., Majtanik, M., … Fink, G. R. (2003). Synchronization Tomography: A Method for Three-Dimensional Localization of Phase Synchronized Neuronal Populations in the Human Brain using Magnetoencephalography. *Physical Review Letters*, *90*(8), 4. https://doi.org/10.1103/PhysRevLett.90.088101

Tesche, C. D., & Karhu, J. (1997). Somatosensory evoked magnetic fields arising from sources in the human cerebellum. *Brain Research*, *744*(1), 23–31. https://doi.org/10.1016/S0006-8993(96)01027-X

Tesche, C. D., & Karhu, J. J. T. (2000). Anticipatory cerebellar responses during somatosensory omission in man. *Human Brain Mapping*, *9*(3), 119–142. https://doi.org/10.1002/(SICI)1097-0193(200003)9:3<119::AID-HBM2>3.0.CO;2-R

Thurling, M., Kahl, F., Maderwald, S., Stefanescu, R. M., Schlamann, M., Boele, H.-J., … Timmann, D. (2015). Cerebellar Cortex and Cerebellar Nuclei Are Concomitantly Activated during Eyeblink Conditioning: A 7T fMRI Study in Humans. *Journal of Neuroscience*, *35*(3), 1228–1239. https://doi.org/10.1523/JNEUROSCI.2492-14.2015

Tierney, T. M., Holmes, N., Meyer, S. S., Boto, E., Roberts, G., Leggett, J., … Barnes, G. R. (2018). Cognitive neuroscience using wearable magnetometer arrays: Non-invasive assessment of language function. *NeuroImage*, *In press*. https://doi.org/10.1016/j.neuroimage.2018.07.035

Timmermann, L., Gross, J., Dirks, M., Volkmann, J., Freund, H. J., & Schnitzler, A. (2003). The cerebral oscillatory network of parkinsonian resting tremor. *Brain*, *126*(1), 199–212. https://doi.org/10.1093/brain/awg022

Todd, N. P. M., Govender, S., & Colebatch, J. G. (2018). The human electrocerebellogram (ECeG) recorded non-invasively using scalp electrodes. *Neuroscience Letters*, *682*(May), 124–131. https://doi.org/10.1016/j.neulet.2018.06.012

Valls-Solé, J., Valldeoriola, F., Molinuevo, J. L., Cossu, G., & Nobbe, F. (1999). Prepulse modulation of the startle reaction and the blink reflex in normal human subjects. *Experimental Brain Research*, *129*(1), 49–56. https://doi.org/10.1007/s002210050935

Yuval-Greenberg, S., Tomer, O., Keren, A. S., Nelken, I., & Deouell, L. Y. (2008). Transient Induced Gamma-Band Response in EEG as a Manifestation of Miniature Saccades. *Neuron*, *58*(3), 429–441. https://doi.org/10.1016/j.neuron.2008.03.027